Engineering 7 (2021) 636–646

Contents lists available at ScienceDirect

Engineering

journal homepage: www.elsevier.com/locate/eng

Research
Green Chemical Engineering: Soft Matter—Article

Functional Capsules Encapsulating Molecular-Recognizable Nanogels for Facile Removal of Organic Micro-Pollutants from Water

Wen-Ying Liu [a], Xiao-Jie Ju [a,b,*], Xing-Qun Pu [a], Quan-Wei Cai [a], Yu-Qiong Liu [a], Zhuang Liu [a,b], Wei Wang [a,b], Rui Xie [a,b], Liang-Yin Chu [a,*]

[a] School of Chemical Engineering & State Key Laboratory of Hydraulics and Mountain River Engineering, Sichuan University, Chengdu 610065, China
[b] State Key Laboratory of Polymer Materials Engineering, Sichuan University, Chengdu 610065, China

ARTICLE INFO

Article history:
Received 11 August 2020
Revised 5 November 2020
Accepted 8 February 2021
Available online 2 April 2021

Keywords:
Functional capsules
Molecular-recognizable nanogels
Organic micro-pollutants
Host–guest complexation
Separations

ABSTRACT

A novel method has been successfully developed for the facile and efficient removal of organic micro-pollutants (OMP) from water based on novel functional capsules encapsulating molecular-recognizable nanogels. The functional capsules are composed of ultrathin calcium alginate (Ca-Alg) hydrogel shells as semipermeable membranes and encapsulated poly(*N*-isopropylacrylamide-*co*-acrylic acid-*g*-mono-(6-ethanediamine-6-deoxy)-β-cyclodextrin) (PNCD) nanogels with β-cyclodextrin (CD) moieties as OMP capturers. The semipermeable membranes of the capsules enable the free transfer of OMP and water molecules across the capsule shells, but confine the encapsulated PNCD nanogels within the capsules. Bisphenol A (BPA), an endocrine-disrupting chemical that is released from many plastic water containers, was chosen as a model OMP molecule in this study. Based on the host–guest recognition complexation, the CD moieties in the PNCD nanogels can efficiently capture BPA molecules. Thus, the facile and efficient removal of BPA from water can be achieved by immersing the proposed functional capsules into BPA-containing aqueous solutions and then simply removing them, which is easily done due to the capsules' characteristically large size of up to several millimeters. The kinetics of adsorption of BPA molecules by the capsules is well described by a pseudo-second-order kinetic model, and the isothermal adsorption thermodynamics align well with the Freundlich and Langmuir isothermal adsorption models. The regeneration of capsules can be achieved simply by washing them with water at temperatures above the volume phase transition temperature of the PNCD nanogels. Thus, the proposed functional capsules encapsulating molecular-recognizable nanogels provide a novel strategy for the facile and efficient removal of OMP from water.

1. Introduction

The global occurrence of organic micro-pollutants (OMP) such as pesticides, pharmaceuticals, and endocrine-disrupting chemicals (EDCs) in water resources results in adverse effects on aquatic ecosystems and human health due to the long-term toxic stimulation of exposed organisms [1–4]. For example, the existence of EDCs throughout the human body can break down the central nervous and endocrine systems by mimicking the biological activity of natural hormones and occupying hormone receptors, which can interfere in the transport and metabolic processes of natural hormones, harming humans and other animals [5–8]. Therefore, the efficient removal of OMP from aquatic systems is of vital significance for the protection of the environment and human health.

Based on interaction mechanisms, chemical reactions [9–12], rejections [13–16], and adsorptions [5,17,18] have been proposed for the removal of OMP from water. As an example of a chemical reaction mechanism, photocatalytic degradation [19–22] can convert OMP into non-toxic inorganic small molecules. In such reactions, the radiation energy absorbed by the photocatalysts induces electron-hole pairs to initiate subsequent redox reactions; however, the reactions are usually limited by the chemical structures of the contaminants and the demand for activating catalysts. Based on rejection mechanisms, reverse osmosis membranes and nano-filtration membranes [13–16] can realize the removal of

* Corresponding authors.
E-mail addresses: juxiaojie@scu.edu.cn (X.-J. Ju), chuly@scu.edu.cn (L.-Y. Chu).

https://doi.org/10.1016/j.eng.2021.02.007

OMP from water with a high retention rate; however, they are limited to a certain extent by the drawbacks of high operating pressures and low permeability [23]. By contrast, due to their simple operation processes, methods based on the mechanisms of chemical or physical adsorption between adsorbents and OMP are widely used for the removal of OMP from water. Affinity membranes for adsorptions and separations, which are generally synthesized by blending [24] or grafting [25,26] functional materials onto substrate membranes, can specifically associate with OMP via the functional materials. Typically, cyclodextrins (CDs) and their derivatives, which contain large ring cavity structures with hydrophilic rims and hydrophobic interiors, can effectively capture typical OMP molecules from water by forming stable host–guest complexes between CDs and OMP molecules [27–29]. Based on such host–guest complexations, porous CD-based polymers have been developed for the rapid removal of OMP from water [30]. By controllably designing the pore structures and increasing the number of effective adsorption sites in the fabricated materials, the removal efficiency of OMP can be increased effectively. However, the separation of the OMP-adsorbed functional polymers from the continuous phase still requires membrane filtration technology, such as the use of microfiltration or ultrafiltration membranes. Unfortunately, membrane filtration processes require membrane modules and usually need frequent membrane-washing procedures, which are time-consuming and troublesome. Therefore, the removal of OMP is still not as facile as desired. High-silica zeolites [31] and carbon materials [32–34], such as activated carbon [33], biochar [32], and mesoporous carbon [34], can also remove OMP based on adsorption mechanisms as a result of their large specific surface areas and unique surface characteristics. However, for the removal of OMP, these methods are non-specific and exhibit performance decay during adsorbent regeneration. Thus far, the facile and efficient removal of OMP from water is still challenging.

Herein, novel functional capsules encapsulating molecular-recognizable nanogels are developed for the facile and efficient removal of OMP from water. The functional capsules are composed of ultrathin calcium alginate (Ca-Alg) hydrogel shells as semipermeable membranes and encapsulated poly(*N*-isopropylacrylamide-*co*-acrylic acid-*g*-mono-(6-ethanediamine-6-deoxy)-β-cyclodextrin) (PNCD) nanogels with β-CD moieties as OMP capturers (Fig. 1(a)). The Ca-Alg hydrogel capsules are controllably fabricated by means of a co-extrusion mini-fluidic technique [35–37]. The molecular-recognizable PNCD nanogels are synthesized by grafting functional mono-(6-ethanediamine-6-deoxy)-β-CD onto poly (*N*-isopropylacrylamide-*co*-acrylic acid) (PNA) nanogels prepared via precipitation polymerization. The semipermeable membranes enable the free transfer of OMP and water molecules across the capsule shells, but confine the encapsulated nanogels within the capsules. Bisphenol A (BPA), an EDC released from plastic water containers [35], was chosen as a model OMP molecule due to its toxicity and widespread existence in water. When the proposed capsules encapsulating nanogels are added to an environmental aqueous solution containing BPA molecules (Fig. 1(b)), the isothermal adsorption of BPA molecules (Figs. 1(a-I) and (b-I)) is achieved by the BPA-recognizable complexation of CD moieties in the encapsulated nanogels. The nanogels inside the capsule exhibit a BPA-induced complexation (Figs. 1(a-II) and (b-II)) due to the formation of host–guest complexes between the CD moieties and BPA molecules (Figs. 1(a-III) and (b-III)). Thus, the facile and efficient removal of BPA from water can be achieved by immersing the proposed functional capsules in BPA-containing aqueous solutions and then simply removing them using sieves with large pores, as the capsules are characterized by a very large size of up to several millimeters. Thus, the proposed method provides a novel strategy for the facile and efficient removal of OMP from water.

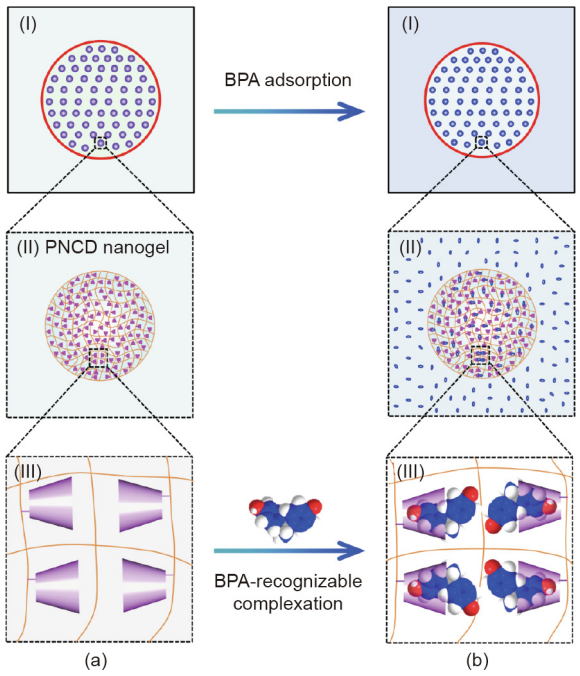

Fig. 1. Schematic illustration of the proposed concept of functional capsules for the facile removal of OMP from water. (a) The capsule is composed of (I) a semipermeable membrane and (II) encapsulated molecular-recognizable nanogels with (III) CD moieties for specifically recognizing bisphenol A (BPA). (b) When the proposed capsules are added to an environmental aqueous solution containing BPA molecules, the isothermal adsorption of (I) BPA molecules is achieved by the BPA-recognizable complexation of CD moieties in the encapsulated nanogels. (a-II, b-II) The nanogels inside the capsule exhibit (a-III, b-III) a BPA-induced complexation due to the formation of host–guest complexes between the CD moieties and BPA. Thus, the removal of BPA from water can be easily achieved.

2. Experimental section

2.1. Materials

Chemical reagents, including ammonium persulfate (APS), *N*,*N*′-methylene-bisacrylamide (MBA), sodium dodecyl sulfate (SDS), acrylic acid (AAc), sodium alginate (Na-Alg), sodium carboxymethylcellulose (CMC), and calcium nitrate ($Ca(NO_3)_2$), were purchased from Chengdu Kelong Chemical Reagent Factory (China). Mono-(6-ethanediamine-6-deoxy)-β-CD was purchased from Shandong Binzhou Zhiyuan Biotechnology Co., Ltd. (China). A solvent mixture of hexane/acetone (50/50, v/v) was used to recrystallize *N*-isopropylacrylamide (NIPAM) (98%; Tokyo Chemical Industry, Japan). 1-(3-(Dimethylamino) propyl)-3-ethylcarbodiimide hydrochloride (EDC) was purchased from Sigma-Aldrich (USA). All other chemicals were of analytical grade and were used as received. Deionized water (18.2 MΩ, 25 °C) purified from a Milli-Q Plus water purification system (Millipore, USA) was used throughout this work.

2.2. Synthesis and characterization of molecular-recognizable PNCD nanogels

The PNCD nanogels with CD moieties as OMP capturers were synthesized with the monomers AAc and NIPAM by means of precipitation copolymerization followed by the grafting of CD moieties onto the copolymer networks [36]. In brief, for the synthesis of the PNA nanogels, AAc (0.4324 g) and NIPAM (2.7158 g) monomers, along with the initiator APS (0.0685 g), the cross-linker MBA (0.1203 g), and the surfactant SDS (0.0091 g), were put into a 300 mL flask with deionized water as the solvent.

The flask was purged with nitrogen gas for 30 min to remove the dissolved oxygen in the solution. After that, the reaction was carried out for 4 h at 70 °C under a nitrogen atmosphere. The solution was then cooled to room temperature using an ice bath. Next, filtration and dialysis against deionized water were carried out to achieve the separation and purification of the PNA nanogels. Finally, to synthesize PNCD nanogels, modification of the PNA nanogels was performed by grafting CD onto the PNA nanogels via a condensation reaction with EDC as the catalyst at 6 °C for 16 h (Figs. S1(a) and (b) in Appendix A).

To confirm the successful synthesis of PNCD nanogels, Fourier-transform infrared spectroscopy (FT-IR; NICOLET iS50; Thermo Scientific, USA) was used for a chemical composition characterization of the CD, PNA nanogels, and PNCD nanogels. The morphology of the PNA and PNCD nanogels was observed using a field- emission scanning electron microscope (FESEM; JSM-7500F; JEOL, Japan). The samples of PNA and PNCD nanogels for the FESEM characterization were sputter-coated with gold after being dried at room temperature.

To demonstrate the complexation of the CD moieties in the PNCD nanogels with the BPA molecules, the temperature-dependent hydrodynamic diameter changes of the PNCD nanogels in pure water and in 0.25 mmol·L^{-1} BPA solution were measured by means of dynamic light scattering (DLS; Zetasizer Nano ZEN3690; Malvern Panalytical Ltd., UK) in aqueous solutions with the temperature changing from 20 to 65 °C. The PNCD nanogel-containing dispersion was highly diluted with deionized water and equilibrated for at least 180 s at each predetermined temperature.

2.3. Fabrication of Ca-Alg functional capsules encapsulating PNCD nanogels

For the fabrication of the Ca-Alg functional capsules, water-in-water (W/W) droplets acting as templates were prepared using a co-extrusion mini-fluidic capillary device, as described in our previous works [37–39] (Figs. S1(c) and (d)). This technology can realize accurate and independent control of the inner and outer phase fluids, enabling accurate control of the size of the droplet templates for fabricating capsule membranes with good monodispersity. The device was fabricated by sleeving a cylindrical capillary tube on a square capillary tube to form a coaxial geometry. The inner diameter of the cylindrical tube was 2.0 mm, and the inner and outer dimensions of the square tube were respectively 1.0 and 1.4 mm. W/W droplets were formed at the outlet of the device by simultaneously injecting the inner fluid into the square tube and the outer fluid through the space between the cylindrical and square tubes via two separate injection pumps (Fig. S1(c)); the volume flow rates of the inner fluid and outer fluid were respectively 40 and 10 mL·h^{-1}. The inner aqueous fluid contained PNCD nanogels and CMC (0.75% w/v), and the outer aqueous fluid contained Na-Alg (2% w/v) and SDS (1% w/v). To make the droplets stable, CMC was added to the inner fluid to increase the viscosity, while SDS was added to the outer fluid as an emulsifier to reduce the interfacial tension between the inner and outer fluids [40]. Nanogel-encapsulated Ca-Alg hydrogel capsules were prepared by continuously dripping the W/W droplets into a $Ca(NO_3)_2$ solution (15% w/v) (Fig. S1(d)). The shell thickness of the Ca-Alg capsules was controlled by tuning the flowrate ratio of the inner fluid to the outer fluid. When the volume flowrate of the outer fluid is constant, the membrane thickness of the Ca-Alg capsules decreases with the increase of the volume flowrate of the inner fluid within a certain range. In contrast, when the volume flowrate of the inner fluid is constant, the membrane thickness of the Ca-Alg capsules increases with the increase of the volume flowrate of the outer fluid. The membrane thickness of the capsules can affect the trans-membrane permeation of the substance. Therefore, the thinner the capsule membrane is, the lower the trans-membrane permeation resistance for BPA will be. To investigate the effect of PNCD content on the BPA adsorption performance, capsules encapsulating different concentrations of PNCD nanogels ([PNCD], w/v) were fabricated by varying the [PNCD] in the inner fluids from 0 to 5, 10, 15, 20, and 30 mg·mL^{-1}. The as-prepared capsules were washed with pure water, and then stored in pure water for subsequent experiments. Optical micrographs were taken with a digital camera for morphology observation, and the monodispersity of the Ca-Alg capsules was characterized with the coefficient of variation (CV) values of the capsule diameters [37,38].

2.4. Determination of the optimal composition of capsules for the removal of BPA from water

To determine the optimum composition of the functional capsules for the removal of BPA from water, the effect of [PNCD] on the BPA adsorption performance of the capsules was investigated. Capsules prepared with 5, 10, 15, 20, and 30 mg·mL^{-1} of PNCD nanogels were respectively placed into a series of glass containers with 2 mL of 0.5 mmol·L^{-1} BPA solution at 25 °C. The number of each type of capsule in a single container varied from 5 to 10, 20, 30, and 40 capsules. The glass containers were placed in a shaker with a thermostatic water bath. To confirm the BPA adsorption effects of the PNCD nanogels, a control group of capsules without encapsulated PNCD nanogels was also tested. The time-dependent concentration change of the BPA solution was monitored by measuring the ultraviolet absorbance of the bulk solution using a micro ultraviolet spectrophotometer (NanoDrop One; Thermo Scientific, USA). A maximum absorption wavelength of λ_{max} = 276 nm was chosen, and a calibration curve correlating the ultraviolet absorbance of the BPA solution and the concentration was established. The removal efficiency of BPA from water (R) by the capsules was determined by the following equation [30]:

$$R = \frac{C_0 - C_t}{C_0} \times 100\% \quad (1)$$

where C_0 (mmol·L^{-1}) and C_t (mmol·L^{-1}) respectively denote the BPA concentrations ([BPA]) in the bulk solution initially and at time t (min).

The mass of BPA adsorbed by the capsules was determined by the following equations [30]:

$$Q_t = (C_0 - C_t)MV \quad (2)$$

$$q_t = \frac{Q_t}{m} \quad (3)$$

where Q_t (mg) denotes the total mass of BPA adsorbed by the capsules at time t (min), q_t (mg·g^{-1}) denotes the amount of BPA adsorbed per gram of PNCD nanogels (dry weight) encapsulated within the capsules at time t (min), M (g·mol^{-1}) is the molar mass of BPA, V (L) denotes the volume of the BPA solution used in the adsorption experiments, and m (g) denotes the total mass of PNCD nanogels used in this study, calculated using the following equation:

$$m = m_1 V_1 N_1 \quad (4)$$

where m_1 (mg·mL^{-1}) denotes the [PNCD] within the capsules, V_1 (L) denotes the inner volume of each capsule, and N_1 denotes the number of capsules used for the adsorption test.

To study the adsorption kinetics, the removal rate of BPA by the capsules can be described by a pseudo-second-order adsorption model, as expressed by the following equation [41,42]:

$$\frac{t}{q_t} = \frac{t}{q_e} + \frac{1}{K_{obs} q_e^2} \quad (5)$$

where q_e (mg·g^{-1}) denotes the mass of BPA adsorbed per gram of PNCD nanogels within the capsules at an equilibrium state, and K_{obs} denotes the apparent second-order rate constant (g·mg^{-1}·min^{-1}).

2.5. Thermodynamics of adsorption of BPA by the capsules

To understand the thermodynamics of the isothermal adsorption of BPA by the capsules, the effect of [BPA] on the BPA adsorption performance of the capsules was investigated. A total of 20 capsules encapsulating 15 mg·mL^{-1} of PNCD nanogels per capsule were placed into each 2 mL BPA solution at 25 °C with the value of [BPA] being respectively 0.025, 0.05, 0.1, 0.3, 0.5, 0.7, and 0.9 mmol·L^{-1}. The time-dependent adsorption mass and removal efficiency of BPA can be determined based on Eqs. (1) and (3). The thermodynamic adsorption mechanism between the Ca-Alg capsules containing functional PNCD nanogels and the BPA molecules was studied using the Langmuir, Freundlich, and Redlich–Peterson adsorption isotherm models, respectively. Three adsorption isotherm models were used to quantitatively analyze the thermodynamic adsorption mechanism. The Langmuir adsorption isotherm can be generated by plotting $1/q_e$ versus $1/C_e$, as follows [25,30]:

$$\frac{1}{q_e} = \frac{1}{q_{max,cal}} + \frac{1}{K_L q_{max,cal}} \cdot \frac{1}{C_e} \tag{6}$$

where $q_{max,cal}$ (mg·g^{-1}) is the theoretical maximum adsorption capacity of the capsules at an equilibrium state, C_e (mmol·L^{-1}) denotes the [BPA] in the bulk solution at the equilibrium state, and K_L is the equilibrium constant.

The Freundlich adsorption isotherm can be generated by plotting $\ln q_e$ versus $\ln C_e$, as follows [25]:

$$\ln q_e = K_F + \frac{1}{n} \ln C_e \tag{7}$$

where K_F and n are the Freundlich constants.

The Redlich–Peterson adsorption isotherm can be generated by plotting C_e/q_e versus C_e, as follows [43]:

$$\frac{C_e}{q_e} = \frac{1}{A} + \frac{B}{A} C_e^{\beta} \tag{8}$$

where A and B are the Redlich–Peterson constants, and β is a coefficient between 0 and 1.

2.6. Thermodynamic behaviors and regeneration tests of capsules

To further study the thermodynamics of BPA adsorption into the functional capsules, the effect of temperature on BPA adsorption performance was investigated. A total of 20 capsules encapsulating 15 mg·mL^{-1} of PNCD nanogels in each capsule were placed into each 2 mL BPA solution at 25, 50, and 60 °C, respectively. These three temperature points were chosen based on the thermo-responsive behavior of PNCD nanogels in BPA-containing solutions, due to the effect of temperature on the interaction between PNCD and BPA. When the PNCD nanogels were immersed in 0.25 mmol·L^{-1} BPA solution, the hydrodynamic diameter of the PNCD nanogels showed nearly no change when the temperature was increased from 20 to 32 °C, indicating that BPA recognition is temperature independent within this temperature range. However, the PNCD nanogels exhibited obvious thermo-responsive volume shrinkage from 32 to 60 °C. When the temperature was increased further, to above 60 °C, the hydrodynamic diameter of the PNCD nanogels remained nearly unchanged. Therefore, 25, 50, and 60 °C were selected as typical temperature points in the experiments. The change in [BPA] in the external solution with time was measured until equilibrium was reached at a predetermined temperature. After that, the Gibbs free energy change (ΔG), enthalpy change (ΔH), and entropy change (ΔS) for the adsorption process were used for the evaluation of thermodynamic behaviors. These parameters can be calculated by the Van't Hoff equations [5,17,44,45]:

$$\ln K_L = \frac{\Delta S}{R_g} - \frac{\Delta H}{R_g T} \tag{9}$$

$$\Delta G = \Delta H - T\Delta S \tag{10}$$

where R_g is the gas constant (8.314 J·mol^{-1}·K^{-1}), T (K) is the temperature of the BPA solution in the adsorption experiments, and ΔH is obtained by calculating the slope of a plot of $\ln K_L$ versus T^{-1}.

To confirm the regeneration characteristics of the capsules, the BPA adsorption–desorption performances of the capsules were investigated. A total of 20 capsules encapsulating 15 mg·mL^{-1} PNCD nanogels in each capsule were placed into each 2 mL BPA solution at 25 °C. The change in [BPA] with time was measured until equilibrium was reached. After that, the BPA solution was substituted over and over with 2 mL of pure water at 50 °C, until the [BPA] in the external solution remained invariant upon the further substitution of pure water. The adsorption of BPA by the capsules and the desorption of BPA from the capsules into pure water were operated for several cycles to investigate the regeneration performance of the capsules. After desorption, the capsules were easily separated from the continuous phase of the BPA solution by means of a simple filter. The desorption efficiency, R_d, was calculated using the following equation:

$$R_d = \frac{Q_d}{Q_e} \times 100\% \tag{11}$$

where Q_d (mg) denotes the total mass of BPA desorbed from the capsules in the washed water after reaching the desorption equilibrium and Q_e (mg) denotes the total mass of BPA adsorbed by the capsules after reaching the adsorption equilibrium.

3. Results and discussion

3.1. Composition and morphology of molecular-recognizable PNCD nanogels

The FT-IR spectra of CD, the PNA nanogels, and the PNCD nanogels are shown in Fig. S2 in Appendix A. Due to the isopropyl groups in NIPAM, double peaks at 1388 and 1368 cm^{-1} can be observed in the FT-IR spectra of both the PNA and PNCD nanogels. The characteristic peak for the carboxylic groups of PNA nanogels at 1716 cm^{-1} disappears after the grafting of CD, indicating that the carboxylic groups have been converted to amide groups via EDC condensation. The characteristic peak for CD at 1034 cm^{-1} is present in the FT-IR spectra of both the CD and the PNCD nanogels. These results confirm the successful synthesis of PNCD nanogels. The scanning electron microscope (SEM) images show that both the PNA nanogels (Fig. S3 in Appendix A) and the PNCD nanogels (Fig. 2(a)) have monodispersed and spherical shapes.

3.2. Molecular-recognition performance of PNCD nanogels

The hydrodynamic diameters of the PNCD nanogels in 0.25 mmol·L^{-1} BPA solution are always smaller than those in pure water at predetermined temperatures (Fig. 2(b)). The decrease in the hydrodynamic diameters of the PNCD nanogels in 0.25 mmol·L^{-1} BPA solution is due to the supramolecular host–guest complexation between the CD moieties and BPA molecules, which results in a slight shrinkage of the hydrogel network (Figs. 1(a-III) and (b-III)) [29,46]. In the complexation, the nonpolar guest BPA molecule partially enters into the hydrophobic cavity of

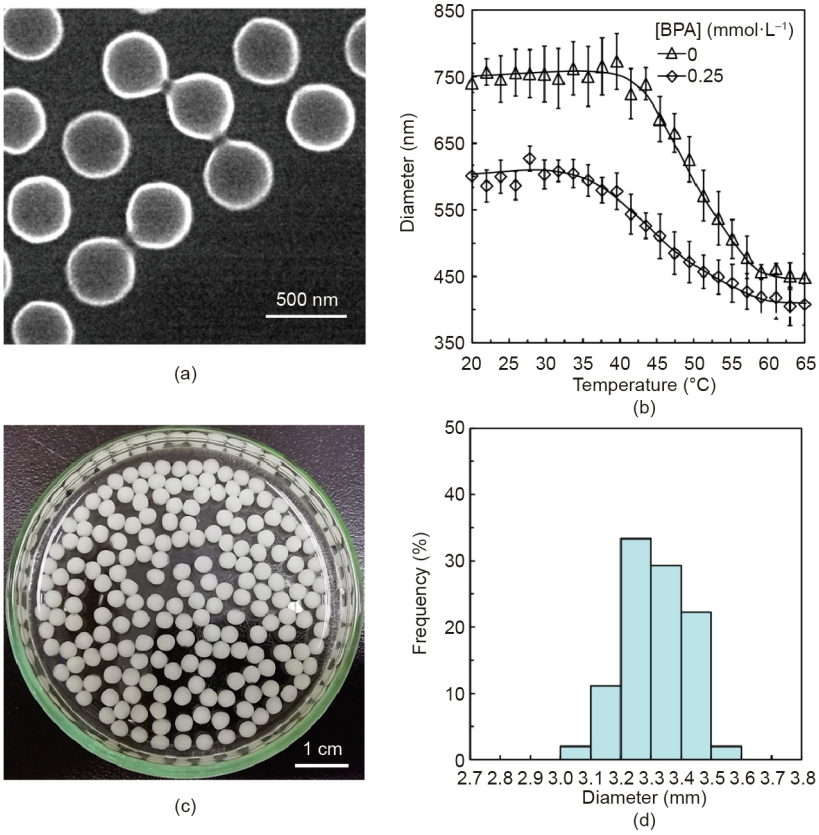

Fig. 2. (a) SEM image of the PNCD nanogels in the dried state; (b) effect of BPA on the hydrodynamic diameters of PNCD nanogels in aqueous solutions at different temperatures; (c) optical micrograph and (d) corresponding size distribution of functional capsules containing 15 mg·mL^{-1} PNCD in each capsule.

the CD unit and forms a stable host–guest CD/BPA inclusion complex via the size effect and supramolecular hydrophobic interaction. In the complexation process, the hydrophobic phenyl group in BPA is exposed outside the cavity of CD, which increases the hydrophobicity of the PNCD nanogels. Therefore, the PNCD nanogels shrink slightly upon capturing BPA molecules. The PNCD nanogels also show thermo-responsive volume changes in both pure water and BPA solution because of the poly(NIPAM) backbones [47,48]. However, within the temperature range of 20–65 °C, regardless of temperature changes, the hydrodynamic diameter of the PNCD nanogels in 0.25 mmol·L^{-1} BPA solution is always smaller than that in pure water, due to the supramolecular host–guest complexation between the CD moieties and BPA molecules that induces a decrease in the hydrophilicity of the PNCD nanogels. The results demonstrate the excellent BPA recognition and adsorption performances of PNCD nanogels.

3.3. Morphological analyses of capsules

The membrane thickness of the Ca-Alg hydrogel capsules decreases with an increase in the ratio of Q_i/Q_o [49], where Q_i and Q_o are the volumetric flow rates of the inner and outer phases. A thin membrane results in a low trans-membrane permeation resistance to BPA transport. To achieve an appropriate thickness of the capsule membrane, Q_i and Q_o were respectively fixed at 40 and 10 mL·h^{-1} in this study. A thin capsule membrane is appropriate because it allows the BPA molecules to pass through the membrane with a low permeation resistance. In addition, the membrane should be robust enough so that the capsules do not rupture during the process. Fig. 2(c) depicts an optical micrograph and Fig. 2(d) shows the size distribution of the prepared capsules encapsulating 15 mg·mL^{-1} of the PNCD nanogels. The capsules are characterized by a uniform spherical morphology and narrow size distribution; the average diameter is around 3.32 mm with a CV value of 3.03%. This high level of monodispersity minimizes the influence of capsule size on adsorption repeatability.

3.4. BPA adsorption characteristics of functional capsules

To determine the optimum capsule composition for BPA adsorption, the effect of the amount of PNCD nanogel within a single capsule and the effect of capsule number on the BPA adsorption characteristics were investigated. Figs. 3(a) and (b) shows the adsorption characteristics of blank capsules without encapsulated PNCD nanogels for removing BPA from a 0.5 mmol·L^{-1} BPA solution at 25 °C. Due to the weak physical adsorption between the Ca-Alg hydrogel capsules and BPA molecules, only a small amount of BPA is adsorbed by the capsules. Both the total mass of BPA adsorbed by the capsules and the removal efficiency increase with an increase in the number of capsules. The total adsorbed mass and removal efficiency of BPA by the capsules are respectively within the ranges of 0.005–0.047 mg and 2.5%–20% for the blank Ca-Alg hydrogel capsules, with the number of capsules ranging from 5 to 40. Remarkably, compared with the adsorption performance of the blank capsules, the BPA adsorption performance of the capsules encapsulating PNCD nanogels is significantly enhanced. For capsules encapsulating 5 mg·mL^{-1} of PNCD nanogels, the time-dependent total mass Q_t (Fig. 3(c)) and removal efficiency R (Fig. 3(d)) at the equilibrium states are respectively within the range of 0.041–0.171 mg and 17.9%–74.8% for a capsule number ranging from 5 to 40. The Q_t and R increase with the increase of time and capsule number, and adsorption equilibrium is reached

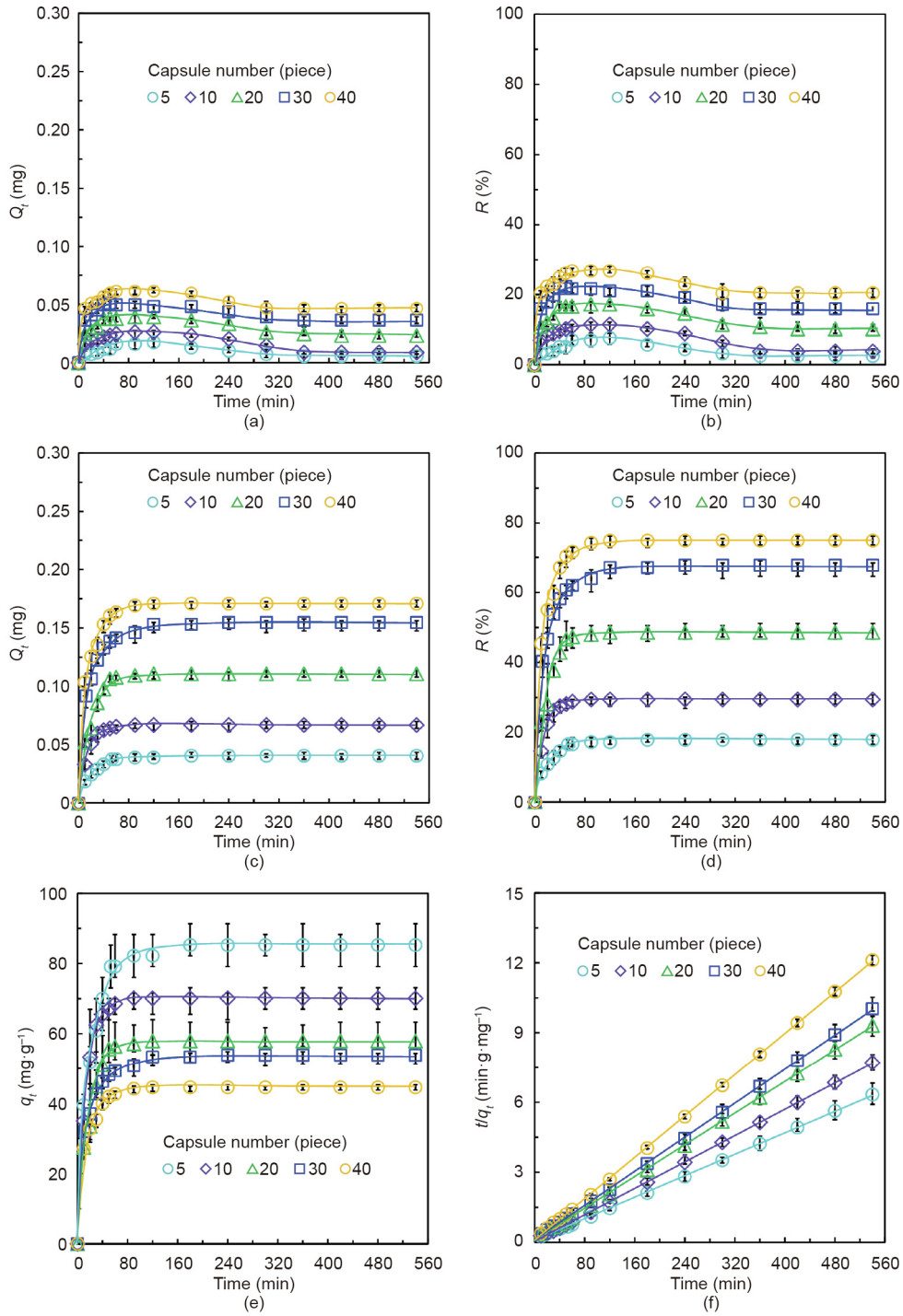

Fig. 3. Adsorption characteristics of different numbers of capsules toward 0.5 mmol·L^{-1} BPA in water at 25 °C. (a) Q_t and (b) R changes in BPA adsorbed by capsules without encapsulated PNCD nanogels. (c) Q_t, (d) R, and (e) q_t changes in BPA adsorbed by capsules encapsulating 5 mg·mL^{-1} of PNCD nanogels in each capsule. (f) Pseudo-second-order plots of BPA adsorbed by capsules encapsulating 5 mg·mL^{-1} PNCD nanogels in each capsule.

within 1 h under these conditions with different numbers of capsules. For each capsule number, q_t decreases with the increase of capsule number (Fig. 3(e)), which means that the amount of adsorbed BPA by a unit mass of PNCD nanogels decreases with an increase of capsule number. This phenomenon aligns with the supposition that the possibility of a BPA molecule being captured by a CD moiety in the PNCD nanogels decreases when the ratio of the amount of CD to BPA increases. Furthermore, the BPA adsorption kinetics data for different numbers of capsules agrees with a pseudo-second-order model (Fig. 3(f)). The results show that, for the adsorption of BPA by capsules encapsulating PNCD nanogels, chemisorption between the adsorption sites of the adsorbents and adsorbates is the rate-limiting step, which confirms that the CD moieties in the encapsulated PNCD nanogels play a leading role in the adsorption of BPA molecules.

For the capsules encapsulating 10 mg·mL^{-1} (Fig. S4 in Appendix A), 15 mg·mL^{-1} (Fig. S5 in Appendix A), 20 mg·mL^{-1} (Fig. S6 in Appendix A), and 30 mg·mL^{-1} (Fig. S7 in Appendix A) of PNCD

nanogels in each capsule, similar changes in Q_t (Figs. S4(a)–S7(a)), R (Figs. S4(b)–S7(b)), and q_t (Figs. S4(c)–S7(c)) were observed over time. The BPA adsorption kinetics also agrees with the pseudo-second-order model (Figs. S4(d)–S7(d)). The total adsorbed mass Q_e and removal efficiency R of BPA increased with an increase in [PNCD] from 0 to 30 mg·mL^{-1} for the conditions with 5 and 10 capsules in the adsorption experiments (Fig. 4). However, when 20, 30, or 40 capsules were present in the adsorption experiments, Q_e and R first increased and then remained nearly invariant with an increase in [PNCD], and the inflection points occurred at about [PNCD] = 15 mg·mL^{-1}. These results indicated that 20 capsules containing 15 mg·mL^{-1} of PNCD nanogels in each capsule would provide the optimum conditions for further investigation of the BPA adsorption characteristics, since 20 capsules provide a BPA removal efficiency of about 80% in 2 mL 0.5 mmol·L^{-1} BPA solution. For each capsule number, the q_e decreases with an increase in [PNCD] (Fig. 4(b)). The greater the [PNCD], the lesser the amount of adsorbed BPA normalized by a unit mass of PNCD nanogels will be. Table S1 in Appendix A shows all the pseudo-second-order plots for the removal of BPA from 0.5 mmol·L^{-1} BPA solution by capsules containing different [PNCD]. The data include the pseudo-second-order model, the K_{obs} (g·mg^{-1}·min^{-1}), the experimental adsorbed mass at the equilibrium state $q_{e,exp}$ (mg·g^{-1}), and the theoretical value according to the model $q_{e,cal}$ (mg·g^{-1}). The results show that the values of $q_{e,exp}$ are almost the same as those of $q_{e,cal}$.

3.5. Adsorption kinetics and thermodynamics of capsules for BPA removal

Capsules containing 15 mg·mL^{-1} PNCD nanogels in each capsule were used to investigate the adsorption kinetics and thermodynamics of BPA removal. For each solution with different [BPA], the Q_t (Fig. 5(a)) and q_t (Fig. 5(b)) of the adsorbed BPA first increased with time and then remained nearly invariant after the adsorption equilibrium was reached. The Q_t and q_t values increased as the [BPA] increased from 0.025 to 0.9 mmol·L^{-1}. More BPA was adsorbed by the capsules in solutions with higher [BPA], which is reasonable, as there were sufficient adsorption sites in the capsules. For a [BPA] of less than 0.5 mmol·L^{-1}, the removal efficiency R (Fig. 5(c)) remained higher than 80%. However, R decreased slightly when the [BPA] was increased further to 0.9 mmol·L^{-1}. When the capsule number is fixed, the adsorption sites provided by the PNCD nanogels are also fixed, regardless of how the [BPA] changes. Therefore, R decreases slightly when the [BPA] increases further. Pseudo-second-order kinetics for BPA adsorption by the capsules were also observed for aqueous solutions with different [BPA] (Fig. 5(d)). Table 1 provides the fitting results of the kinetics parameters and demonstrates that the pseudo-second-order model is more suitable for solutions with higher [BPA]. Furthermore, the Freundlich, Langmuir, and Redlich–Peterson isothermal adsorption models were used to describe the isothermal adsorption thermodynamics for BPA adsorption by the capsules. The fitting results show that both the Freundlich (Fig. 5(e)) and Langmuir (Fig. 5(f)) isothermal adsorption models can be used to describe the BPA adsorption very well, with coefficients of association, R^2, of 0.9936 and 0.9921, respectively. However, the Freundlich isothermal adsorption model was found to be more suitable than the Langmuir isothermal adsorption model because the association coefficient of the Freundlich model is slightly larger than that of Langmuir model. In comparison, the R^2 value is only 0.9398 for the Redlich–Peterson isothermal adsorption model (Fig. S8 in Appendix A). These fitting results for the adsorption data further reveal that the adsorption mechanism of the capsules against BPA molecules is a multilayer adsorption mechanism in an inhomogeneous surface that is dominated by chemisorption, due to the complexation between CD and BPA [30,50], with assistance from physisorption. Thus, the adsorption is inhomogeneous. Moreover, the value of n in the Freundlich isothermal adsorption model is equal to 1.15, which means that the adsorption of BPA by the capsules is favorable.

Furthermore, the results from the additional investigations of the adsorption thermodynamics of BPA at 25, 50, and 60 °C by capsules containing 15 mg·mL^{-1} of PNCD nanogels in each capsule showed that the adsorptions at different temperatures agree quite well with both the Freundlich (Fig. 6(a)) and Langmuir (Fig. 6(b)) isothermal adsorption models. For the adsorption of BPA from aqueous solutions with [BPA] increasing from 0.1 to 0.9 mmol·L^{-1}, the removal efficiency R of BPA (Fig. 6(c)) decreased slightly at each fixed temperature. At a fixed [BPA], the R value decreased as the temperature increased from 25 to 60 °C. When the environmental temperature increases, the poly(NIPAM) backbones in the PNCD nanogels shrink, resulting in an increase in the steric hindrance of the PNCD hydrogel networks and a decrease in the complexation constant between the CD and BPA molecules. As a result, the effective amount of BPA complexed with CD in the PNCD nanogels decreases with increasing temperature. To further investigate the adsorption behavior of BPA by the capsules, the temperature-dependent adsorption was determined; the results are shown in a Van't Hoff plot (Fig. 6(d)) along with the thermodynamic parameters, including Gibb's free energy change ΔG < 0 kJ·mol^{-1}, enthalpy change ΔH = −5407.7 J·mol^{-1}, and entropy change ΔS = 50.83 J·mol^{-1}·K^{-1}. The negative value of ΔH indicates the exothermic nature of BPA adsorption, which is supported by the decline in the removal efficiency of BPA with increasing temperature. Furthermore, the positive value of ΔS

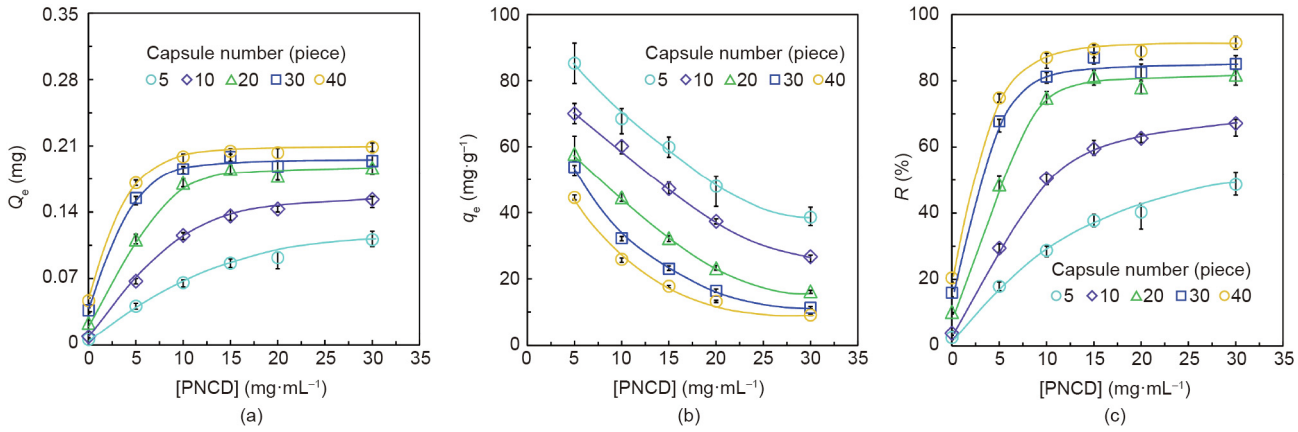

Fig. 4. Effect of the [PNCD] within capsules on the adsorption of 0.5 mmol·L^{-1} BPA in water at 25 °C: (a) Q_e; (b) q_e; and (c) R.

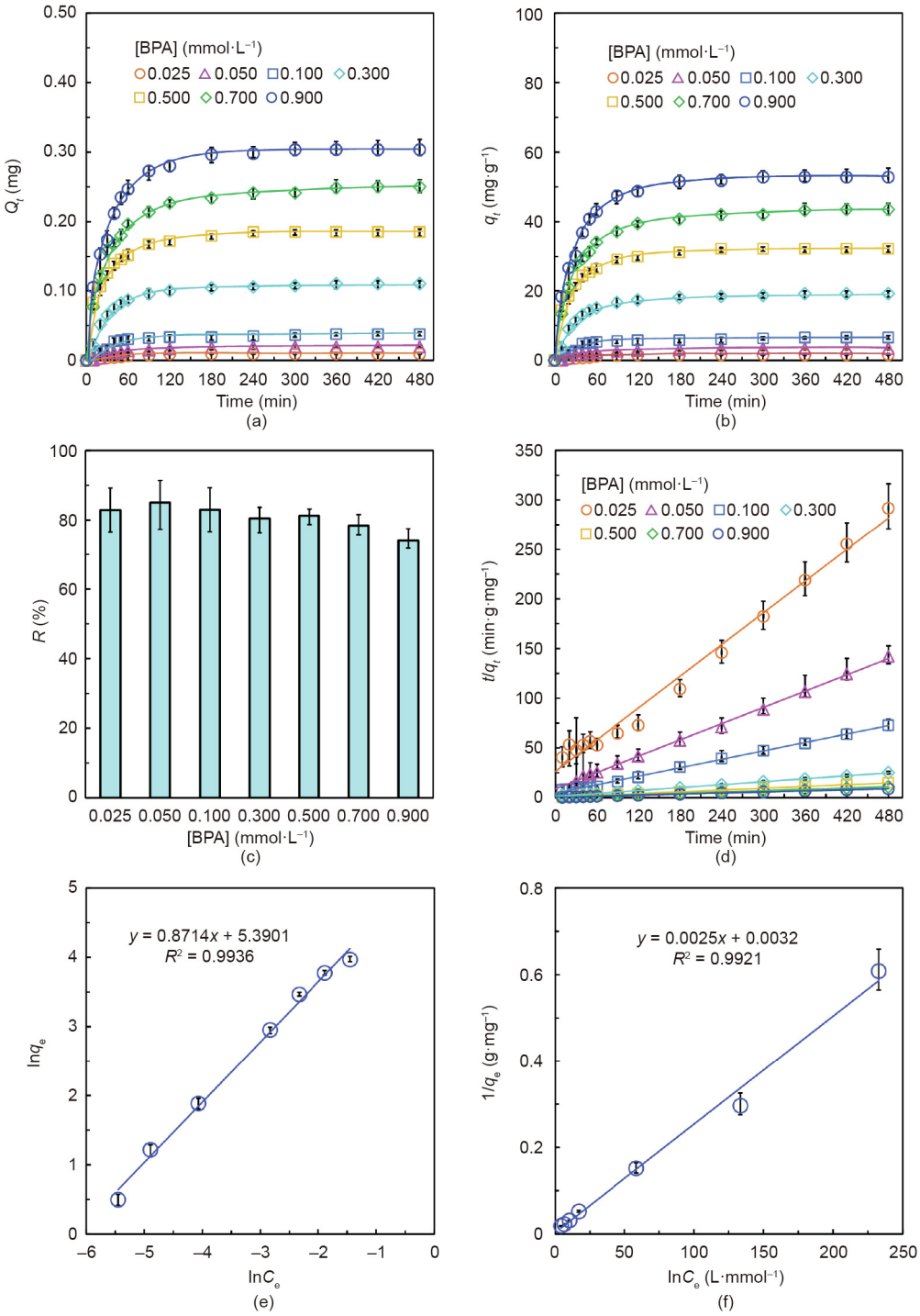

Fig. 5. Adsorption characteristics of 20 capsules containing 15 mg·mL^{-1} of PNCD nanogels in each capsule for the adsorption of BPA in aqueous solutions with different [BPA] at 25 °C. (a) Q_t and (b) q_t changes in the BPA adsorbed by 20 capsules in aqueous solutions. (c) R and (d) pseudo-second-order plots of the BPA adsorbed by the capsules in aqueous solutions. (e) Freundlich and (f) Langmuir isothermal adsorption model fittings of the BPA adsorption data.

reveals that the overall adsorption process of BPA by the capsules involves an increase in entropy. As shown in Table 2, ΔG indicates that the adsorptions are spontaneous processes.

3.6. Regeneration characteristics of capsules for BPA removal

After BPA adsorption, capsule regeneration is conducted by simply washing the capsules with deionized water at temperatures higher than the volume phase transition temperature (VPTT) of the PNCD nanogels. Adsorption/regeneration of the capsules is performed for five cycles, with adsorption at 25 °C in the BPA solution and desorption at 50 °C in deionized water (Fig. 7). The adsorption–desorption mechanism is based on the synergistic effect of the thermo-responsive and molecular-recognizable performances of the PNCD nanogels (Fig. 7(a)). When the temperature is lower than the VPTT (at 25 °C in this study), the hydrogel networks of the PNCD nanogels are in a hydrophilic and swollen state, and the CD moieties and BPA molecules can form stable host–guest

Table 1
Pseudo-second-order plot results of BPA adsorption by capsules containing 15 mg·mL^{-1} of PNCD nanogels per capsule in aqueous solutions with different [BPA].

[BPA] (mmol·L^{-1})	Pseudo-second-order model	R^2	$q_{e,exp}$ (mg·g^{-1})	$q_{e,cal}$ (mg·g^{-1})	K_{obs} (g·mg^{-1}·min^{-1})
0.025	y = 0.5321x + 26.347	0.9874	1.6446	1.8793	0.0108
0.050	y = 0.2728x + 8.9563	0.9987	3.3764	3.6657	0.0083
0.100	y = 0.1415x + 4.5261	0.9963	6.5858	7.0671	0.0044
0.300	y = 0.0492x + 1.2303	0.9984	19.1696	20.3252	0.0020
0.500	y = 0.0298x + 0.5574	0.9994	32.0074	33.5571	0.0016
0.700	y = 0.0219x + 0.4746	0.9998	43.5747	45.6621	0.0010
0.900	y = 0.0180x + 0.3358	0.9996	52.8549	55.5556	0.0010

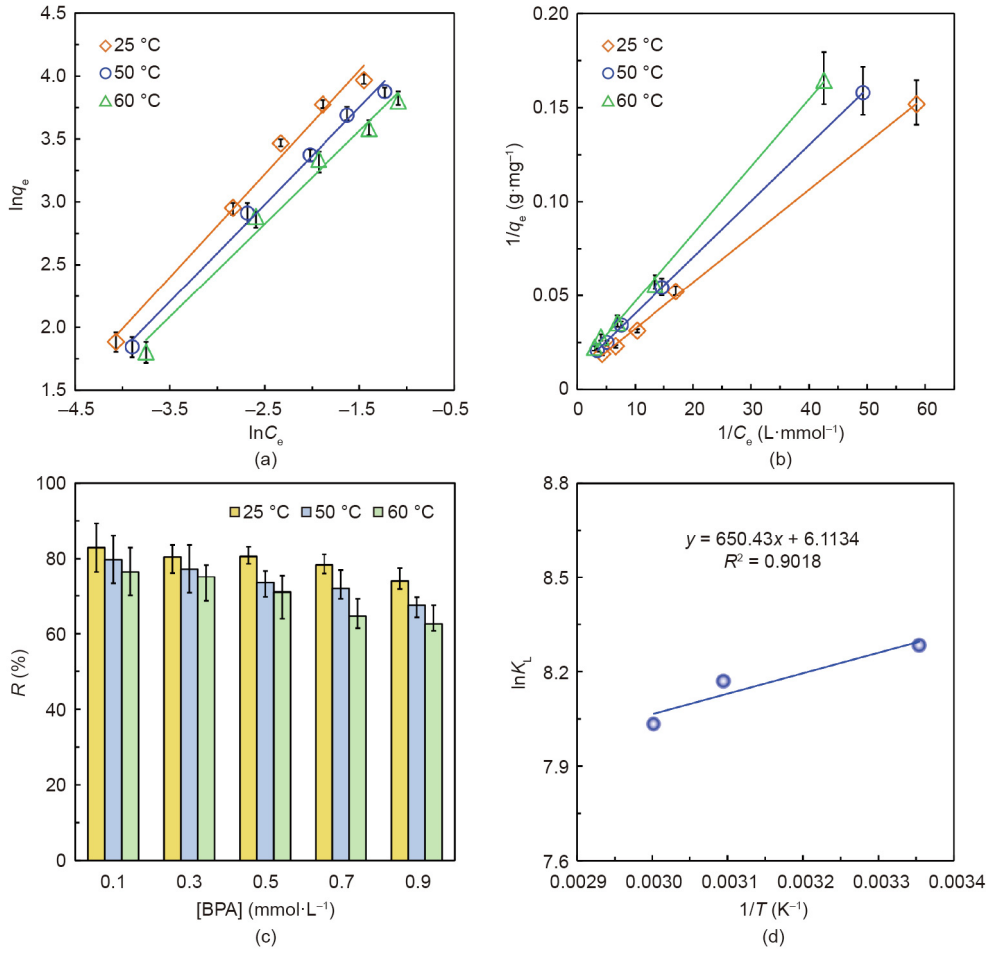

Fig. 6. Adsorption thermodynamics of capsules containing 15 mg·mL^{-1} PNCD nanogels in each capsule toward BPA. (a) Freundlich and (b) Langmuir isothermal adsorption models fitting the BPA adsorption data at 25, 50, and 60 °C. (c) R and (d) Van't Hoff plot for BPA adsorption by the capsules.

Table 2
Thermodynamic parameters for the adsorption of BPA by capsules containing 15 mg·mL^{-1} PNCD nanogels in each capsule at 25, 50, and 60 °C.

T (K)	lnK_L	ΔG (kJ·mol^{-1})
298.15	8.2835	−20.5617
323.15	8.1700	−21.8324
333.15	8.0337	−22.3406

complexes (Fig. 7(a-I)). However, when the temperature increases to higher than the VPTT (at 50 °C in this study), the hydrogel networks of the PNCD nanogels change to a hydrophobic and shrunken state, and the complexation constant between the CD and BPA molecules decreases [46]; thus, the desorption of BPA molecules from the CD moieties becomes easier (Fig. 7(a-II)). The desorbed BPA molecules permeate through the Ca-Alg hydrogel shell of the capsules outward into the external water under the driving force of the concentration difference between the internal and external environment. The results show that the functional capsules exhibit excellent desorption performances in each cycle, and the desorption efficiency R_d can be maintained at around 90% (Figs. 7(b) and (c)). Meanwhile, the removal efficiency of BPA by the capsules only slightly decreases after six adsorption–desorption cycles. In short, the capsules possess excellent regeneration characteristics and can be used repeatedly by washing away the adsorbed BPA with deionized water at temperatures above the VPTT of the PNCD nanogels. Under general conditions, the Ca-Alg shell of the prepared capsules can maintain good stability in water for several months at least. However, due to the protonation or deprotonation of carboxyl groups in alginate chains, strong acid or alkali aqueous solutions can cause the degradation of Ca-Alg hydrogel shells. Even though the released nanogels can interact

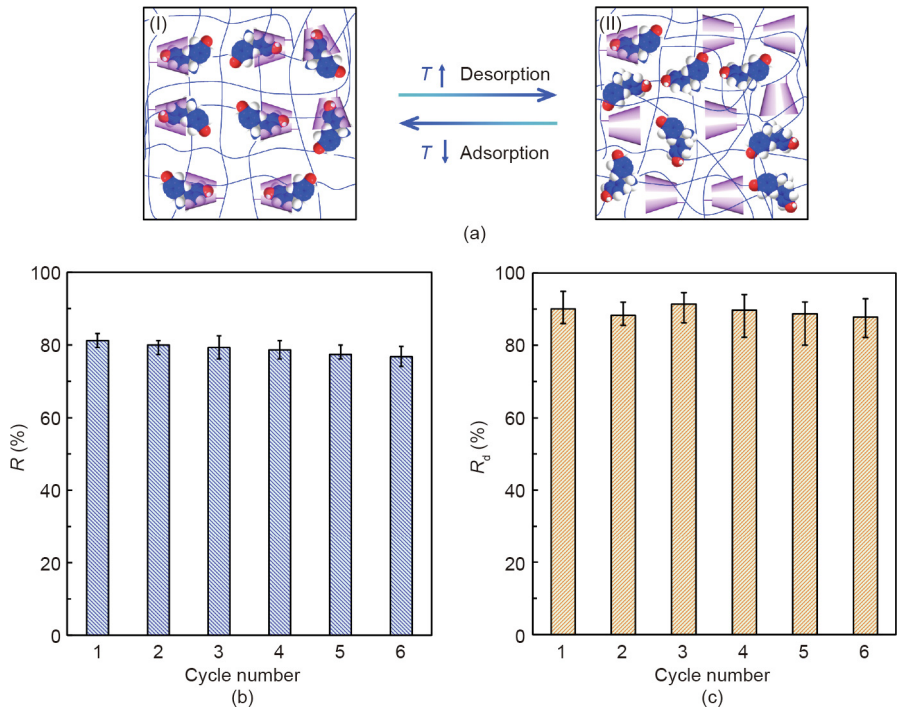

Fig. 7. Adsorption–desorption performances of capsules containing 15 mg·mL^{-1} PNCD nanogels in each capsule toward BPA. (a) Schematic illustration of the adsorption–desorption of BPA molecules by the CD moieties based on the synergistic thermo-responsive and molecular-recognizable properties of the PNCD nanogels, showing (I) adsorption at 25 °C and (II) desorption at 50 °C. (b) *R* and (c) R_d of capsules toward 0.5 mmol·L^{-1} BPA under six cycles of repeated adsorption at 25 °C and desorption at 50 °C.

directly with the targets, the post-treatment for separating the nanogel adsorbents from the medium is difficult. Therefore, pure water provides the most appropriate storage conditions for the functional capsules.

4. Conclusions

In summary, a novel method has been successfully developed for the facile and efficient removal of OMP from water based on novel functional capsules containing molecular-recognizable PNCD nanogels. The functional capsules are composed of semipermeable membranes and encapsulated PNCD nanogels with BPA-recognizable CD moieties. The semipermeable membranes of the capsules enable the free transfer of BPA and water molecules across the capsule shells, but confine the encapsulated PNCD nanogels within the capsules. Based on host–guest recognition complexation, the CD moieties in the PNCD nanogels can efficiently capture BPA molecules. In this way, the facile and efficient removal of BPA from water can be achieved by immersing the proposed functional capsules into BPA-containing aqueous solutions and then simply removing them, which is easily done because the capsules are characterized by a very large size of up to several millimeters. The prepared capsules exhibit excellent removal efficiency toward BPA, and the equilibrium removal efficiency increases with an increase of the concentration of the encapsulated PNCD nanogels in each capsule and the number of capsules. The adsorption kinetics of the BPA molecules by the capsules can be well described by a pseudo-second-order kinetic model, and the isothermal adsorption thermodynamics agree with the Freundlich and Langmuir isothermal adsorption models. The adsorption of BPA molecules by the capsules is mainly due to the chemisorption of BPA via complexation between CD and BPA molecules, and the adsorption process is an exothermic one with an increase in entropy. Capsule regeneration can be achieved by simply washing the capsules with deionized water at temperatures above the VPTT of the PNCD nanogels. The proposed method based on functional capsules containing molecular-recognizable nanogels provides a novel strategy for the facile and efficient removal of OMP from water.

Acknowledgement

The authors gratefully acknowledge support from the National Natural Science Foundation of China (21991101).

Compliance with ethics guidelines

Wen-Ying Liu, Xiao-Jie Ju, Xing-Qun Pu, Quan-Wei Cai, Yu-Qiong Liu, Zhuang Liu, Wei Wang, Rui Xie, and Liang-Yin Chu declare that they have no conflict of interest or financial conflicts to disclose.

Appendix A. Supplementary data

Supplementary data to this article can be found online at https://doi.org/10.1016/j.eng.2021.02.007.

References

[1] Schwarzenbach RP, Escher BI, Fenner K, Hofstetter TB, Johnson CA, von Gunten U, et al. The challenge of micropollutants in aquatic systems. Science 2006;313(5790):1072–7.
[2] Anh HQ, Tomioka K, Tue NM, Tuyen LH, Chi NK, Minh TB, et al. A preliminary investigation of 942 organic micro-pollutants in the atmosphere in waste processing and urban areas, northern Vietnam: levels, potential sources, and risk assessment. Ecotoxicol Environ Saf 2019;167:354–64.
[3] Eggen RIL, Hollender J, Joss A, Schärer M, Stamm C. Reducing the discharge of micropollutants in the aquatic environment: the benefits of upgrading wastewater treatment plants. Environ Sci Technol 2014;48(14):7683–9.
[4] Hollender J, Zimmermann SG, Koepke S, Krauss M, McArdell CS, Ort C, et al. Elimination of organic micropollutants in a municipal wastewater treatment plant upgraded with a full-scale post-ozonation followed by sand filtration. Environ Sci Technol 2009;43(20):7862–9.

[5] Xu J, Wang L, Zhu Y. Decontamination of bisphenol A from aqueous solution by graphene adsorption. Langmuir 2012;28(22):8418–25.
[6] Chang HS, Choo KH, Lee B, Choi SJ. The methods of identification, analysis, and removal of endocrine disrupting compounds (EDCs) in water. J Hazard Mater 2009;172(1):1–12.
[7] Ternes TA, Stumpf M, Mueller J, Haberer K, Wilken RD, Servos M. Behavior and occurrence of estrogens in municipal sewage treatment plants—I. investigations in Germany, Canada and Brazil. Sci Total Environ 1999;225(1–2):81–90.
[8] Kloas W, Lutz I, Einspanier R. Amphibians as a model to study endocrine disruptors: II. estrogenic activity of environmental chemicals *in vitro* and *in vivo*. Sci Total Environ 1999;225(1–2):59–68.
[9] Dao KC, Yang CC, Chen KF, Tsai YP. Recent trends in removal pharmaceuticals and personal care products by electrochemical oxidation and combined systems. Water 2020;12(4):1043.
[10] Xu Y, Liu T, Zhang Y, Ge F, Steel RM, Sun L. Advances in technologies for pharmaceuticals and personal care products removal. J Mater Chem A Mater Energy Sustain 2017;5(24):12001–14.
[11] Tay KS, Rahman NA, Radzi Bin Abas M. Kinetic studies of the degradation of parabens in aqueous solution by ozone oxidation. Environ Chem Lett 2010;8(4):331–7.
[12] Xu L, Wang J. Magnetic nanoscaled Fe_3O_4/CeO_2 composite as an efficient Fenton-like heterogeneous catalyst for degradation of 4-chlorophenol. Environ Sci Technol 2012;46(18):10145–53.
[13] Ouyang Z, Huang Z, Tang X, Xiong C, Tang M, Lu Y. A dually charged nanofiltration membrane by pH-responsive polydopamine for pharmaceuticals and personal care products removal. Separ Purif Technol 2019;211:90–7.
[14] Zangeneh H, Zinatizadeh AA, Zinadini S, Feyzi M, Bahnemann DW. Preparation and characterization of a novel photocatalytic self-cleaning PES nanofiltration membrane by embedding a visible-driven photocatalyst boron doped-TiO_2–SiO_2/$CoFe_2O_4$ nanoparticles. Separ Purif Technol 2019;209:764–75.
[15] Wang J, Zhu J, Tsehaye MT, Li J, Dong G, Yuan S, et al. High flux electroneutral loose nanofiltration membranes based on rapid deposition of polydopamine/polyethyleneimine. J Mater Chem A Mater Energy Sustain 2017;5(28):14847–57.
[16] Radjenović J, Petrović M, Ventura F, Barceló D. Rejection of pharmaceuticals in nanofiltration and reverse osmosis membrane drinking water treatment. Water Res 2008;42(14):3601–10.
[17] Fu J, Chen Z, Wang M, Liu S, Zhang J, Zhang J, et al. Adsorption of methylene blue by a high-efficiency adsorbent (polydopamine microspheres): kinetics, isotherm, thermodynamics and mechanism analysis. Chem Eng J 2015;259:53–61.
[18] Rizzo L, Fiorentino A, Grassi M, Attanasio D, Guida M. Advanced treatment of urban wastewater by sand filtration and graphene adsorption for wastewater reuse: effect on a mixture of pharmaceuticals and toxicity. J Environ Chem Eng 2015;3(1):122–8.
[19] Xu J, Li L, Guo C, Zhang Y, Meng W. Photocatalytic degradation of carbamazepine by tailored $BiPO_4$: efficiency, intermediates and pathway. Appl Catal B 2013;130–131:285–92.
[20] Yuan F, Hu C, Hu X, Wei D, Chen Y, Qu J. Photodegradation and toxicity changes of antibiotics in UV and UV/H_2O_2 process. J Hazard Mater 2011;185(2–3):1256–63.
[21] Zhang R, Sun P, Boyer TH, Zhao L, Huang CH. Degradation of pharmaceuticals and metabolite in synthetic human urine by UV, UV/H_2O_2, and UV/PDS. Environ Sci Technol 2015;49(5):3056–66.
[22] Rosenfeldt EJ, Linden KG. Degradation of endocrine disrupting chemicals bisphenol A, ethinyl estradiol, and estradiol during UV photolysis and advanced oxidation processes. Environ Sci Technol 2004;38(20):5476–83.
[23] Schrotter JC, Bozkaya-Schrotter B. Current and emerging membrane processes for water treatment. Membr Technol 2010;4:53–91.
[24] Rana D, Narbaitz RM, Garand-Sheridan AM, Westgate A, Matsuura T, Tabe S, et al. Development of novel charged surface modifying macromolecule blended PES membranes to remove EDCs and PPCPs from drinking water sources. J Mater Chem A Mater Energy Sustain 2014;2(26):10059–72.
[25] Chen ZH, Liu Z, Hu JQ, Cai QW, Li XY, Wang W, et al. β-Cyclodextrin-modified graphene oxide membranes with large adsorption capacity and high flux for efficient removal of bisphenol A from water. J Membr Sci 2020;595:117510.
[26] Kim JH, Park PK, Lee CH, Kwon HH. Surface modification of nanofiltration membranes to improve the removal of organic micro-pollutants (EDCs and PhACs) in drinking water treatment: graft polymerization and cross-linking followed by functional group substitution. J Membr Sci 2008;321(2):190–8.
[27] Zhang YM, Xu QY, Liu Y. Molecular recognition and biological application of modified β-cyclodextrins. Sci China Chem 2019;62(5):549–60.
[28] Yamaguchi H, Kobayashi Y, Kobayashi R, Takashima Y, Hashidzume A, Harada A. Photoswitchable gel assembly based on molecular recognition. Nat Commun 2012;3(1):603.
[29] Takashima Y, Hatanaka S, Otsubo M, Nakahata M, Kakuta T, Hashidzume A, et al. Expansion-contraction of photoresponsive artificial muscle regulated by host–guest interactions. Nat Commun 2012;3(1):1270.
[30] Alsbaiee A, Smith BJ, Xiao L, Ling Y, Helbling DE, Dichtel WR. Rapid removal of organic micropollutants from water by a porous β-cyclodextrin polymer. Nature 2016;529(7585):190–4.
[31] Jiang N, Shang R, Heijman SGJ, Rietveld LC. High-silica zeolites for adsorption of organic micro-pollutants in water treatment: a review. Water Res 2018;144:145–61.
[32] Oliveira FR, Patel AK, Jaisi DP, Adhikari S, Lu H, Khanal SK. Environmental application of biochar: current status and perspectives. Bioresour Technol 2017;246:110–22.
[33] Rodriguez E, Campinas M, Acero JL, Rosa MJ. Investigating PPCP removal from wastewater by powdered activated carbon/ultrafiltration. Water Air Soil Pollut 2016;227:177.
[34] Sui Q, Huang J, Liu Y, Chang X, Ji G, Deng S, et al. Rapid removal of bisphenol A on highly ordered mesoporous carbon. J Environ Sci 2011;23(2):177–82.
[35] Le HH, Carlson EM, Chua JP, Belcher SM. Bisphenol A is released from polycarbonate drinking bottles and mimics the neurotoxic actions of estrogen in developing cerebellar neurons. Toxicol Lett 2008;176(2):149–56.
[36] Yan PJ, He F, Wang W, Zhang SY, Zhang L, Li M, et al. Novel membrane detector based on smart nanogels for ultrasensitive detection of trace threat substances. ACS Appl Mater Interfaces 2018;10(42):36425–34.
[37] Wang JY, Jin Y, Xie R, Liu JY, Ju XJ, Meng T, et al. Novel calcium-alginate capsules with aqueous core and thermo-responsive membrane. J Colloid Interface Sci 2011;353(1):61–8.
[38] He F, Mei L, Ju XJ, Xie R, Wang W, Liu Z, et al. pH-responsive controlled release characteristics of solutes with different molecular weights diffusing across membranes of Ca-alginate/protamine/silica hybrid capsules. J Membr Sci 2015;474:233–43.
[39] He F, Wang W, He XH, Yang XL, Li M, Xie R, et al. Controllable multicompartmental capsules with distinct cores and shells for synergistic release. ACS Appl Mater Interfaces 2016;8(13):8743–54.
[40] Bremond N, Santanach-Carreras E, Chu LY, Bibette J. Formation of liquid-core capsules having a thin hydrogel membrane: liquid pearls. Soft Matter 2010;6(11):2484–8.
[41] Liu YM, Ju XJ, Xin Y, Zheng WC, Wang W, Wei J, et al. A novel smart microsphere with magnetic core and ion-recognizable shell for Pb^{2+} adsorption and separation. ACS Appl Mater Interfaces 2014;6(12):9530–42.
[42] Ho YS, McKay G. Pseudo-second order model for sorption processes. Process Biochem 1999;34(5):451–65.
[43] Redlich O, Peterson DL. A useful adsorption isotherm. J Phys Chem 1959;63(6):1024.
[44] Xin X, Wei Q, Yang J, Yan L, Feng R, Chen G, et al. Highly efficient removal of heavy metal ions by amine-functionalized mesoporous Fe_3O_4 nanoparticles. Chem Eng J 2012;184:132–40.
[45] Pan L, Zhai G, Yang X, Yu H, Cheng C. Thermosensitive microgels-decorated magnetic graphene oxides for specific recognition and adsorption of Pb(II) from aqueous solution. ACS Omega 2019;4(2):3933–45.
[46] Yang M, Chu LY, Xie R, Wang C. Molecular-recognition-induced phase transitions of two thermo-responsive polymers with pendent β-cyclodextrin groups. Macromol Chem Phys 2008;209(2):204–11.
[47] Ju XJ, Liu L, Xie R, Niu CH, Chu LY. Dual thermo-responsive and ion-recognizable monodisperse microspheres. Polymer 2009;50(3):922–9.
[48] Xiong W, Wang W, Wang Y, Zhao Y, Chen H, Xu H, et al. Dual temperature/pH-sensitive drug delivery of poly(*N*-isopropylacrylamide-*co*-acrylic acid) nanogels conjugated with doxorubicin for potential application in tumor hyperthermia therapy. Colloids Surf B Biointerfaces 2011;84(2):447–53.
[49] Liu WY, Ju XJ, Faraj Y, He F, Peng HY, Liu YQ, et al. Capsule membranes encapsulated with smart nanogels for facile detection of trace lead(II) ions in water. J Membr Sci 2020;613:118523.
[50] Dong Y, Wu D, Chen X, Lin Y. Adsorption of bisphenol A from water by surfactant-modified zeolite. J Colloid Interface Sci 2010;348(2):585–90.